Journal of Solid State Chemistry 186 (2012) 104–108

Contents lists available at SciVerse ScienceDirect

Journal of Solid State Chemistry

journal homepage: www.elsevier.com/locate/jssc

$Li_2B_3O_4F_3$, a new lithium-rich fluorooxoborate

Thomas Pilz, Hanne Nuss, Martin Jansen *

Max Planck Institute for Solid State Research, Heisenbergstraße 1, 70569 Stuttgart, Germany

ARTICLE INFO

Article history:
Received 18 October 2011
Accepted 30 November 2011
Available online 8 December 2011

Keywords:
Lithium fluorooxoborate
Lithium ion conductivity
Acentric borate

ABSTRACT

The new lithium fluorooxoborate, $Li_2B_3O_4F_3$, is obtained by a solid state reaction from $LiBO_2$ and $LiBF_4$ at 553 K and crystallizes in the acentric orthorhombic space group $P2_12_12_1$ (no. 19) with the cell parameters $a=4.8915(9)$, $b=8.734(2)$, and $c=12.301(2)$ Å. Chains of fluorinated boroxine rings along the b axis consists of BO_3 triangles and BO_2F_2 as well as BO_3F tetrahedra. Mobile lithium ions are compensating the negative charge of the anionic chain, in which the fourfold coordinated boron atoms bear a negative formal charge. Annealing $Li_2B_3O_4F_3$ at temperatures above 573 K leads to conversion into $Li_2B_6O_9F_2$. The title compound is an ionic conductor with the highest ion conductivity among the hitherto know lithium fluorooxoborates, with conductivities of 1.6×10^{-9} and 1.8×10^{-8} S cm^{-1} at 473 and 523 K, respectively.

1. Introduction

Many oxoborates feature pronouncedly anisotropic oligomeric or polymeric anions, and show a certain inclination to assume non-centrosymmetric space group symmetries. The set of special physical properties related to acentric structures have nourished significant interest in this class of compounds, which includes top performing SHG materials, among others LiB_3O_5 (LBO) [1] and $CsLiB_6O_{10}$ (CLBO) [2].

Recently, we have started investigating alkali fluorooxoborates, with a twofold motivation. (1) Adding a fluoride ion to boron in a threefold planar coordination would shift negative charge to the central boron atom, now in fourfold coordination, thus reducing partial negative charge at the respective terminal oxygen and/or fluorine atoms, which commonly act as pinning sites for the cations. By this measure we aim at enhancing e.g. lithium ion mobility in lithium borates. (2) Including electronegative fluorine would increase the anisotropy of charge distribution within the borate anions, which might improve the SHG, piezoelectric or pyroelectric performance, in general.

By the examples of LiB_6O_9F [3] and $Li_2B_6O_9F_2$ [4] we have demonstrated that lithium fluorooxoborates are accessible by an acid–base reaction in the solid state, where boron oxide or oxoborates with boron in threefold coordination may serve as acids, and LiF or $LiBF_4$ as fluoride bases.

Indeed, all lithium fluorooxoborates discovered are acentric, and show non-linear optical properties, LiB_6O_9F even with an efficiency comparable to KDP [5], they furthermore are pure lithium ion conductors. However, the conductivities found are too low for warranting any application. Since the commonly used approach to increase the charge carrier concentration in ionic conductors by aliovalent doping has failed for lithium fluorooxoborates, so far, we have moved on by synthesizing species with higher stoichiometric Li contents. Here we present the new $Li_2B_3O_4F_3$.

2. Experimental

2.1. Synthesis

All reactions were carried out in purified argon atmosphere using standard Schlenk techniques. $LiBO_2$ (lithium metaborate, anhydrous, Fischer Scientific, reagent grade) was dried at 673 K under vacuum for 4 days. Tetrahydrofurane (Merck, $>99\%$) was dried with sodium and freshly distilled prior to use.

$LiBO_2$ and $LiBF_4$ (Sigma Aldrich, anhydrous, ultra dry 99.998%) were mixed in a ratio of 2:1 and thoroughly ground. The mixture was placed in closed silver crucibles, sealed in glass ampoules and heated from room temperature to 553 K at a heating rate of 100 K/h. After holding the reaction mixture at 553 K for 500 h, it was finally cooled to room temperature at a rate of 1 K/h. The reaction product contained LiF and $Li_2B_3O_4F_3$ in the ratio of 1:2. In order to remove the byproduct, LiF is transformed into $LiBF_4$ by stirring the reaction products in a solution of boron trifluoride tetrahydrofuran complex (50%, Acros Organics) in absolute tetrahydrofurane at room temperature for 3 days. By subsequent filtering, the pure fluorooxoborate was obtained as an insoluble residue.

2.2. Characterization

Powder X-ray diffraction patterns were recorded at room temperature on a high resolution X-ray diffractometer (D8

* Corresponding author. Fax: +49 711 689 1502.
E-mail address: M.Jansen@fkf.mpg.de (M. Jansen).

0022-4596/$ - see front matter © 2011 Elsevier Inc. All rights reserved.
doi:10.1016/j.jssc.2011.11.053

ADVANCE, Bruker AXS, Karlsruhe, Germany) using Cu–$K\alpha$ radiation (Ge(1 1 1)—monochromator). The samples were sealed under argon in a glass capillary with a diameter of 0.5 mm. Diffraction patterns were collected between 5° and 95° 2θ for 14 h. The lattice constants, $a=4.8915(9)$, $b=8.734(2)$, $c=12.301(2)$ Å, were determined from a Le Bail fit [6] using TOPAS [7].

For structure determination, a colorless crystal, suitable for single-crystal X-ray diffraction, was placed on top of a glass fiber and sealed within a glass capillary in a glove box.

Intensity data were collected at 298 K on a SMART-APEX CCD X-ray diffractometer (Bruker AXS Inc., Karlsruhe, Germany) with Mo–$K\alpha$ radiation ($\lambda=0.71073$ Å) and a graphite monochromator. A semi-empirical absorption correction was applied using SADABS [8]. The structure was solved with direct methods and refined using the program package SHELXTL [9]. Further details of the crystal structure investigation are available from the Fachinformationszentrum Karlsruhe, D-76344 Eggenstein-Leopoldshafen (Germany), on quoting the depository number CSD-423661, the name of the authors, and citation of the paper.

Details of single crystal measurement, atom coordinates and displacement parameters are given in Tables 1–3.

The cavity calculations have been performed using the program ATOMSV6.3 [10].

Infrared spectra were recorded between 400 and 4000 cm^{-1} using the FT-IR spectrometer IFS 113v (Bruker Optic, Karlsruhe). Sample pellets were prepared by pressing a thoroughly ground mixture of 300 mg dry KBr and 1 mg sample.

Ionic conductivity was measured from a compact pressed powder pellet (diameter 6 mm; thickness 0.65 mm), placed between two silver electrodes in a quartz tube, floated with argon. The Novocontrol Alpha A 4.2 Analyzer was used with the ZG-4 interface in an 2-wire arrangement. Spectra were recorded from 1 Hz up to 5 MHz during continuous heating at a rate of 0.5 K/min, controlled by WinDeta program [11]. All parameters including σ_{bulk}, Q and n were calculated using the WinFit program [12].

Table 1
Crystal data and structure refinement for $Li_2B_3O_4F_3$.

Empirical formula	**$Li_2B_3O_4F_3$**
Formula weight	167.31
Temperature	298(2) K
Wavelength	0.71073 Å
Crystal system	orthorhombic
Space group	$P2_12_12_1$ (no. 19)
Unit cell dimensions	$a=4.8915(9)$ Å
	$b=8.734(2)$ Å
	$c=12.301(2)$ Å
Volume	525.5(2) $Å^3$
Z	4
Density (calculated)	2.115 g cm^{-3}
Absorption coefficient	0.235 mm^{-1}
$F(0\,0\,0)$	320
Crystal size	$0.20\times0.18\times0.10$ mm^3
Theta range for data collection	2.86–27.49°
Index ranges	$-6\le h\le6$, $-11\le k\le11$, $-15\le l\le15$
Reflections collected	5480
Independent reflections	1216 [R(int)=0.0485]
Completeness to theta=27.49°	100.0%
Max. and min. transmission	0.9769 and 0.9545
Refinement method	Full-matrix least-squares on F^2
Data/restraints/parameters	1216/0/109
Goodness-of-fit on F^2	0.961
Final R indices [$I>2$sigma(I)]	$R1=0.0347$, w$R2=0.0664$
R indices (all data)	$R1=0.0568$, w$R2=0.0726$
Absolute structure parameter	−0.2(10)
Largest diff. peak and hole	0.233 and −0.232 e$Å^{-3}$

Table 2
Atomic coordinates (10^4) and equivalent isotropic displacement parameters ($Å^2\cdot10^3$) for $Li_2B_3O_4F_3$. U(eq) is defined as one third of the trace of the orthogonalized U^{ij} tensor.

Atom	***x***	***y***	***z***	***U*(eq)**
Li(1)	4142(9)	6452(4)	3966(3)	23(1)
Li(2)	16,593(9)	2063(5)	5718(3)	27(1)
B(1)	10,814(5)	3182(3)	6600(2)	16(1)
B(2)	9080(6)	5316(3)	5385(2)	18(1)
B(3)	10,214(5)	5792(3)	7303(2)	17(1)
O(1)	9647(3)	3734(2)	5595(1)	20(1)
O(2)	9582(4)	6339(2)	6289(1)	22(1)
O(3)	10,596(3)	4266(2)	7483(1)	18(1)
O(4)	10,526(3)	6742(2)	8176(1)	20(1)
F(1)	10,710(3)	5798(2)	4477(1)	29(1)
F(2)	6352(3)	5505(2)	5033(1)	27(1)
F(3)	13673(3)	2879(2)	6448(1)	31(1)

Table 3
Anisotropic displacement parameters ($Å^2\cdot10^3$) for $Li_2B_3O_4F_3$. The anisotropic displacement factor exponent takes the form: $-2\pi^2[h^2\,a^{*2}U^{11}+\cdots+2\,h\,k\,a^*\,b^*\,U^{12}]$.

Atom	***U*^{11}**	***U*^{22}**	***U*^{33}**	***U*^{23}**	***U*^{13}**	***U*^{12}**
Li(1)	31(3)	19(2)	19(2)	1(2)	1(2)	1(2)
Li(2)	26(2)	31(2)	23(2)	−5(2)	−3(2)	1(2)
B(1)	18(1)	14(1)	15(1)	−1(1)	−1(1)	−1(1)
B(2)	19(2)	16(1)	17(1)	1(1)	−2(1)	−1(1)
B(3)	16(1)	15(1)	19(1)	1(1)	2(1)	0(1)
O(1)	32(1)	14(1)	14(1)	−1(1)	−4(1)	2(1)
O(2)	33(1)	11(1)	20(1)	0(1)	−6(1)	3(1)
O(3)	29(1)	12(1)	15(1)	−1(1)	−2(1)	2(1)
O(4)	28(1)	12(1)	18(1)	−1(1)	−5(1)	3(1)
F(1)	33(1)	33(1)	22(1)	7(1)	6(1)	−6(1)
F(2)	23(1)	30(1)	29(1)	1(1)	−6(1)	4(1)
F(3)	21(1)	36(1)	36(1)	−8(1)	2(1)	5(1)

3. Results and discussion

3.1. Synthesis

$Li_2B_3O_4F_3$ was synthesized from $LiBO_2$ and $LiBF_4$ at 553 K (Eq. (1)). Pure phase material was obtained after the extraction of the byproduct LiF with dilute $THF\cdot BF_3$.

$$2LiBO_2+LiBF_4\rightarrow Li_2B_3O_4F_3+LiF \quad (1)$$

Annealing of the fluorooxoborate at temperatures higher than 573 K leads to the formation of $Li_2B_6O_9F_2$, which decomposes at 753 K [4]. Solid state reaction of the starting materials $LiBO_2$ and $LiBF_4$, in an appropriate ratio at 623–673 K will directly result in $Li_2B_6O_9F_2$ [4].

3.2. Crystal structure

$Li_2B_3O_4F_3$ crystallizes in the orthorhombic space group $P2_12_12_1$ (no. 19) with two formula units per unit cell. The structure is built of ${}^1_\infty[B_3O_4F_3]^{2-}$ chains running along b and two crystallographically independent, fourfold coordinated Li^+ cations (Fig. 1a). In Fig. 1b, a cutout of the structure shows fluorinated boroxine rings, $[B_3O_4F_3]^{2-}$, bonded to each other via a bridging oxygen atom. Thereby, always a threefold boron atom of one ring (B3) is connected to a fourfold coordinated boron (B1) of another, bearing three O atoms (two ring atoms and one terminal O) and one F atom as nearest neighbors. The third ring-B-atom (B2), not involved in the setup of the chains, is

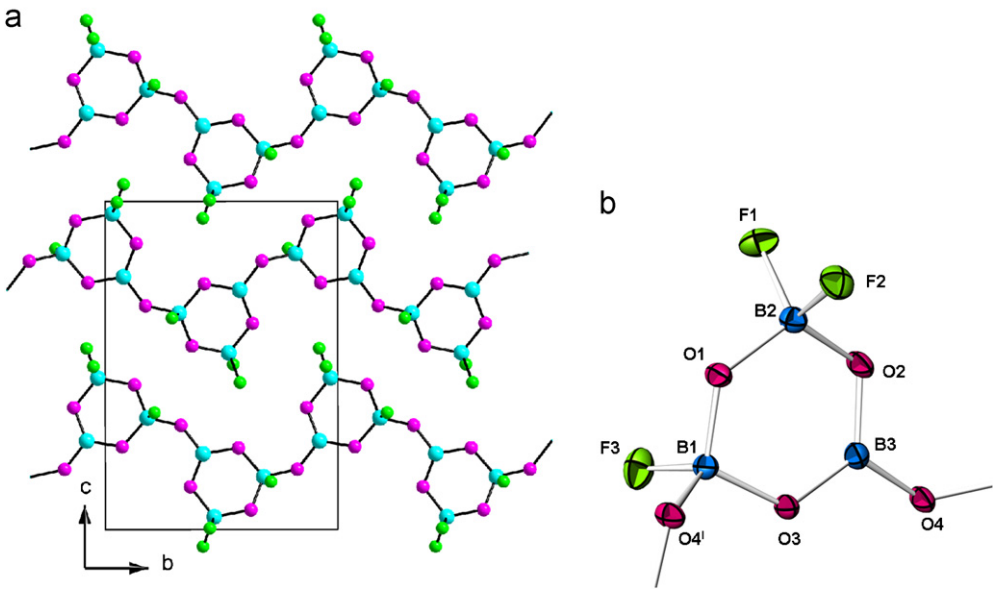

Fig. 1. (a) Projection of the orthorhombic cell in the *bc* plane: chains of the anionic matrix are along the *b* axis. (b) The fundamental building block consists of one trigonal planar BO_3 unit, one tetrahedral BO_2F_2 as well as a tetrahedral BO_3F unit.

Table 4
Selected bond lengths/Å and angles/deg. of the boroxine backbone. Symmetry codes: (I) $-x+2$, $y-1/2$, $-z+3/2$; (II) $x-1$, y, z; (III) $-x+3/2,-y+1$, $z+3/2$; (IV) $x-1/2$, $-y+3/2$, $-z+1$; (V) $x-3/2$, $-y+1/2$, $-z+1$; (VI) $-x+3$, $y-1/2$, $-z+3/2$; (VII) $x+1/2$, $-y+1/2$, $-z+1$; (VIII) $x+3/2$, $-y+1/2$, $-z+1$.

Atom contact	Distance	Atom contact	Angle
B1–F3	1.436(3)	F3–B1–O1	109.6(2)
B1–O1	1.444(3)	F3–B1–O3	106.9(2)
B1–O3	1.444(3)	F3–B1–O4^{I}	107.9(2)
B1–O4^{I}	1.445(3)	O1–B1–O3	113.3(2)
		O1–B1–O4^{I}	105.6(2)
B2–F1	1.435(3)	O3–B1–O4^{I}	113.2(2)
B2–F2	1.412(3)		
B2–O1	1.433(3)	F1–B2–O1	108.4(2)
B2–O2	1.448(3)	F1–B2–O2	108.8(2)
		F2–B2–O1	110.5(2)
B3–O2	1.371(3)	F2–B2–O2	108.9(2)
B3–O3	1.364(3)	F1–B2–F2	104.6(2)
B3–O4	1.365(3)	O1–B2–O2	115.0(2)
		O2–B3–O3	121.3(2)
		O2–B3–O4	121.9(2)
		O3–B3–O4	116.8(2)

bonded to two ring-O atoms and two terminal F atoms. Table 4 summarizes selected bond lengths and angles. The mean *d*(B–O) distance of the ring-B–O bonds within the $[B_3O_4F_3]^{2-}$ units is 1.417 Å, with the B–O bonds involving threefold coordinated boron being significantly shorter (average: 1.368 Å) than those including fourfold bonded B (av.: 1.442 Å). All distances are in good agreement with reported data for borates [13–17] tetrafluoroborates [18,19] and lithium fluorooxoborates [3,4]. The boroxine ring exhibits a twisted-boat conformation with the maximum dihedral angle B3–O3–B1–O1 = 20.96°, as expected by insertion of tetrahedrally coordinated B and in accordance with the fluorinated boroxine ring found in LiB_6O_9F [3] and the interconnected boroxine rings of $Li_2B_6O_9F_2$ [4].

The geometry of the BO_3F unit resembles the similar building block found in LiB_6O_9F [3]. Compared to the latter, the mean O–B–O angle = 110.8° and the mean O–B–F angle = 108.1° approaching more closely that of the ideal tetrahedron and no significant difference in B–O and B–F bond lengths within experimental standard deviations is observed (Table 4). The mean O–B–O angle of the BO_3 triangle is 120.0°, whereby the largest deviation of 3.2° is observed for the bridging oxygen atom O4 (O3–B3–O4).

Table 5
Coordination geometry around lithium (symmetry codes as given in Table 1).

Atom contact	Distance	Atom contact	Angle
Li1–F1^{II}	1.881(4)	F1^{II}–Li1–F2	98.4(2)
Li1–F2	1.891(4)	F1^{II}–Li1–O3^{III}	106.0(2)
Li1–O2^{IV}	1.966(4)	F2–Li1–O3^{III}	118.4(2)
Li1–O3^{III}	1.933(4)	F1^{II}–Li1–O2^{IV}	116.7(2)
		F2–Li1–O2^{IV}	118.5(2)
Li1…Li2^{V}	3.336(6)	O3^{III}–Li1–O2^{IV}	99.2(2)
Li2–F3	1.832(4)	F3–Li2–O4^{VI}	105.8(2)
Li2–O1^{VII}	2.000(4)	F3–Li2–O1^{VII}	99.2(2)
Li2–O1^{II}	2.094(4)	O4^{VI}–Li2–O1^{VI}	147.7(2)
Li2–O4^{VI}	1.979(4)	F3–Li2–O1^{II}	108.7(2)
		O4^{VI}–Li2–O1^{II}	68.9(1)
Li2…Li1^{VIII}	3.335(6)	O1^{VII}–Li2–O1^{II}	121.6(2)
Li2…Li2^{VII}	3.112(5)		

In contrast to the two other fluorooxoborates mentioned above, the title compound exhibits an additional structural feature, a BO_2F_2 tetrahedron incorporated into the ring (Fig. 1b). The O–B–O, O–B–F and F–B–F angles of this building block lie in the expected range, with the F–B–F angle of 104.6(2)° exhibiting the smallest value. For significant deviation from the ideal tetrahedral angle one can discuss several reasons, as e.g. the reduced mutual repulsion of the terminal, strongly electronegative fluorine atoms or an evasive movement due to embedding into a ring-like arrangement. In case of $Li_2B_3O_4F_3$ we attribute the angular distortion mainly to the latter, since the F–B–F angles of BO_2F_2 tetrahedra not included in boroxine rings, as found in $Li_2B_6O_9F_2$ [4] and $(C_2H_{10}N_2)(BPO_4F_2)$ [20], have close to ideal tetrahedral angles.

The B–O and B–F bond lengths are comparable to those in the BO_3F tetrahedron, whereby one of the B–F bonds, *d*(B2–F2) = 1.412(3) Å, is significantly shorter than the other B–F contacts within the structure. The value of about 1.41 Å resembles to the B–F bonds found for BO_2F_2 tetrahedra in the recently reported new acentric fluorooxoborate $Li_2B_6O_9F_2$ [4]. In this compound, however, the BO_2F_2 unit is not part of the boroxine ring, but isolated, showing B–F distances of 1.407(2) Å.

Besides the boroxine backbone, the unit cell contains two crystallographically independent lithium cations, interconnecting the chains. Table 5 summarizes the coordination geometry around lithium, indicating a distorted tetrahedral coordination of Li^+. As can be seen from Fig. 2, the lithium cations are surrounded by two F and two O (Li1), and three O and one F atom (Li2), respectively, in both cases connecting three adjacent $^1_\infty[B_3O_4F_3]^{2-}$ chains. Looking at the space-filling model of $Li_2B_3O_4F_3$ on the left in Fig. 3, it is obvious that the structure is not densely packed, and is displaying channels along *b*. The small white spots, in this, indicate the Li^+ positions within the structure at room temperature. The lithium cations occupy pockets along the chains that exhibit the best coordination with respect to the donor atoms O and F. However, the distances to the channel centers are small, and at elevated temperatures a diffusion along the channels might become possible. In Fig. 3 right, cavities within the unit cell are shown, which are accessible by particles with a radius of about 0.7 Å ($0.65 \leq r(Li^+) \leq 0.76$ Å, depending on the coordination number). Since these cavities

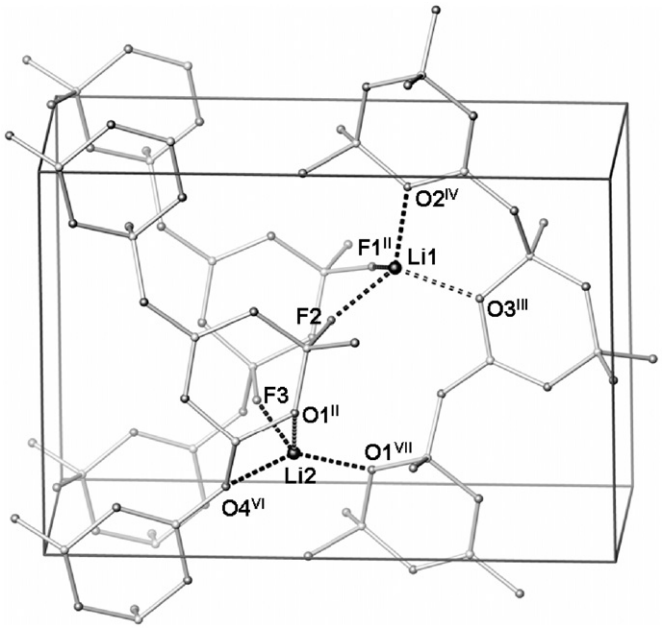

Fig. 2. Tetrahedrally coordinated lithium atoms.

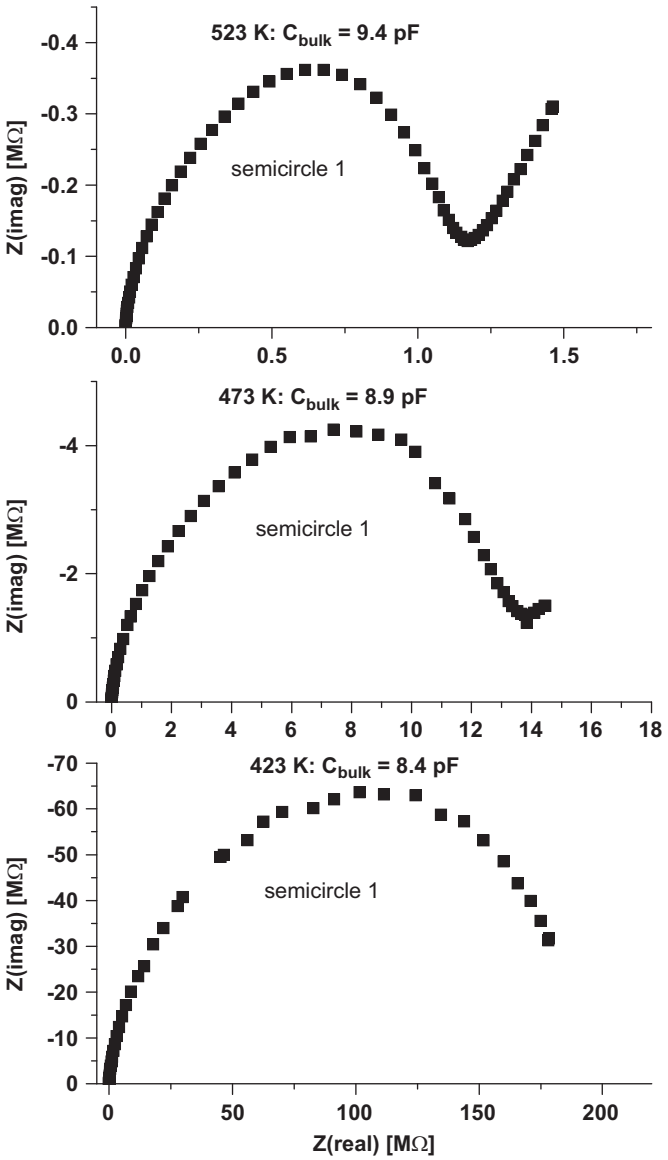

Fig. 4. Nyquist plots for 423, 473 and 523 K obtained from impedance measuremnt of $Li_2B_3O_4F_3$.

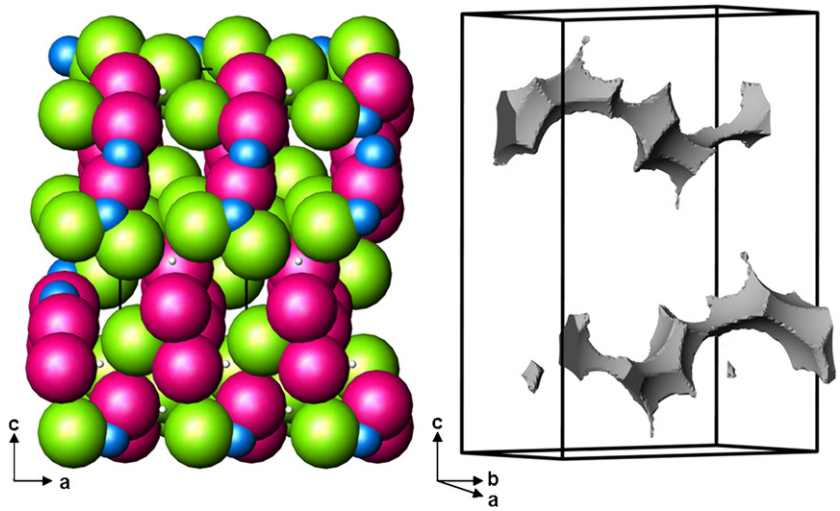

Fig. 3. Left: space-filling representation of the structure using van-der-Waals radii for all non-metal atoms; little white spots indicate the Li^+ positions; right: cavities big enough for particles with a radius of 0.7 Å, calculated with ATOMSV6.3 [10].

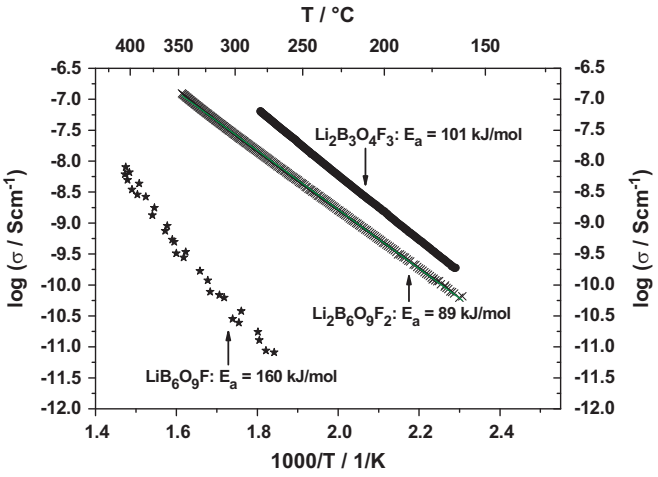

Fig. 5. Arrhenuis plots of lithium fluorooxoborates: obviously the ionic conductivity increases from LiB_6O_9F [3] to $Li_2B_6O_9F_2$ [4] to $Li_2B_3O_4F_3$ (this work).

form continuous channels, they provide possible pathways for ion conduction. The closest intermolecular $Li^+ \ldots Li^+$ distance within this structure is 3.112(5) Å between Li2 and $Li2^{VII}$, which is the closest Li…Li distance found within fluorooxoborates by now.

Hydroxoborates with analogous composition $^1_\infty[B_3O_4X_3]^{2-}$ (X=OH) are colemanite $CaB_3O_4(OH)_3 \cdot H_2O$ [21,22] and hydroboracite $CaMg[B_3O_4(OH)_3]_2 \cdot 3H_2O$ [23]. The anionic repetition units are identical with the fluorooxborate, and can be mutually transformed by replacing fluorine with the hydroxo-group and vice versa.

3.3. Ionic conductivity

The ionic conductivity, bulk capacitance and activation energy for ionic conduction of $Li_2B_3O_4F_3$ was determined by impedance spectroscopy. Data were recorded by heating a pressed pellet of the powdered sample up to 553 K at a rate of 0.5 K/min.

Fig. 4 represents the imaginary part of the impedance plotted versus the real part (so called Nyquist plot) for different temperatures. The semicircle I can be described as an ohmic resistor in parallel to a constant phase element Q, where the latter represents the capacitance C and the "roughness" of the pressed powder, n, according to $C=Q^{1/n} \cdot R^{(1/n)-1}$ (ideal capacitor: $n=1$, $C=Q$). In the hole temperature range the values for n are approximately 0.7.

Compared to our previous reported lithium fluorooxoborates LiB_6O_9F and $Li_2B_6O_9F_2$, $Li_2B_3O_4F_3$ exhibits the highest lithium ion conductivity (Fig. 5).

We attribute this to the increased volumetric density of lithium ions of latter compared to the former.

3.4. IR spectroscopy

For $Li_2B_3O_4F_3$ the spectrum was recorded from 400 to 4000 cm^{-1}, with vibration bands exclusively appearing between 416 and 1435 cm^{-1}, thus presence of hydroxyl group can be convincingly excluded. Strong vibration bands originate from asymmetric stretching modes (ν_{as}) of terahedrally surrounded, and from symmetric stretching modes (ν_s) of trigonally surrounded boron [24]. The assignment was performed in agreement to literature values of tetrafluoroborates [25], lithiumtriborate [26] and other borates [24]. IR(KBr, cm^{-1}): 1435, 1336 (m) ($\nu_{as}B_{(3)}$–O); 1226 (m) (ν(ring)); 1047, 1035 (s) ($\nu_{as}B_{(4)}$–O,F); 941 (s) ($\nu_sB_{(3)}$–O) , 827, 798 (w) ($\nu_sB_{(4)}$–O,F); 727, 698, 675 (w) (bending ($B_{(3)}$–O) out of plane ; 567, 546, 442, 416 (w–m) (further deformation bands).

4. Conclusion

$Li_2B_3O_4F_3$ is the third member among the new family of lithium fluorooxoborates. It consists of one BO_3F and one BO_2F_2 tetrahedron as well as one trigonal planar BO_3 group as a primary building unit. We have attributed the improved Li ion conductivity of $Li_2B_6O_9F_2$ compared to LiB_6O_9F to the higher amount of lithium [4]: this view receives support by the results obtained in the recent work.

References

[1] C. Chen, Y. Wu, A. Jiang, B. Wu, G. You, R. Li, S. Lin, J. Opt. Soc. Am. B 6 (1989) 616–621.
[2] Y. Mori, I. Kuroda, S. Nakajima, T. Sasaki, S. Nakai, Appl. Phys. Lett. 67 (1995) 1818–1820.
[3] G. Cakmak, J. Nuss, M. Jansen, Z. Anorg. Allg. Chem. 635 (2009) 631–636.
[4] T. Pilz, M. Jansen, Z. Anorg. Allg. Chem. 637 (2011) 1–6.
[5] B. Andriyevsky, K. Doll, G. Cakmak, M. Jansen, A. Niemer, K. Betzler, Phys. Rev. B, in press.
[6] A. Le Bail, H. Duroy, J.L. Fourquent, Mater. Res. Bull. 23 (1988) 447.
[7] A.A. Coelho, TOPAS—Graphics based profile and structure analysis software, Version 4.2, Bruker AXS, Inc., Madison, USA, 2010.
[8] G.M. Sheldrick, SADABS—Bruker AXS areas detector scaling and adsorbtion, version 2007/4, University of Göttingen, Germany, 2007.
[9] G.M. Sheldrick, Acta Cryst. Sect. A 64 (2008) 112–122.
[10] E. Dowty, ATOMS—a complete program for displaying atomic structures, version 6.3.4, Shape Software, Kingsport, USA, 2008.
[11] Novocontrol GmbH, WinDeta Version 5.69, Hundsangen, Germany, 2009.
[12] Novocontrol GmbH, WinFit Version 3.2, Hundsangen, Germany, 2005.
[13] H. König, R. Hoppe, Z. Anorg. Allg. Chem. 439 (1978) 71–79.
[14] M. Jansen, G. Brachtel, Nature 67 (1980) 606-606.
[15] H. König, R. Hoppe, M. Jansen, Z. Anorg. Allg. Chem. 449 (1979) 91–101.
[16] M. Schläger, R. Hoppe, Z. Anorg. Allg. Chem. 620 (1994) 1867–1871.
[17] S. Schmid, W. Schnick, Acta Crystallogr., Sect. C: Cryst. Struct. Commun. 60 (2004) 169–170.
[18] K. Matsumoto, R. Hagiwara, Z. Mazej, E. Goreshnik, B. Aemva, J. Phys. Chem. B 110 (2006) 2138–2141.
[19] Z. Mazej, E. Goreshnik, K. Hironaka, Y. Katayama, R. Hagiwara, Z. Anorg. Allg. Chem. 635 (2009) 2309–2315.
[20] Y.-X. Huang, G. Schäfer, H. Borrmann, J.-T. Zhao, R. Kniep, Z. Anorg. Allg. Chem. 629 (2003) 3–5.
[21] C.L. Christ, J.R. Clark, H.T.J. Evans, Acta Cryst. 11 (1958) 761–770.
[22] P.C. Burns, F.C. Hawthorne, Can. Mineral. 31 (1993) 297–304.
[23] C. Sabelli, A. Stoppioni, Can. Mineral. 16 (1978) 75–80.
[24] L. Jun, X. Shuping, G. Shiyang, Spectrochim. Acta, Part A 51 (1995) 519–532.
[25] R.A. Nyquist, R.O. Kagel, Handbook of Infrared and Raman Spectra of Inorganic Compounds and Organic Salts, Vol. 4, Academic Press, San Diego, 1971.
[26] G. Xiong, G. Lan, H. Wang, C. Huang, J. Raman Spectrosc. 24 (1993) 785–789.